Monatshefte für Chemie 135, 1305–1317 (2004)
DOI 10.1007/s00706-004-0216-4

Monatshefte für Chemie
Chemical Monthly
Printed in Austria

Syntheses, Crystal Structures, and Conformations of 10,10-Spiro-Bilirubins

Brahmananda Ghosh, Vincent J. Catalano, and **David A. Lightner***

Department of Chemistry, University of Nevada, Reno, Nevada 89557-0020, USA

Received April 19, 2004; accepted April 26, 2004
Published online July 23, 2004

Summary. Crystal structure determinations of two novel bilirubin analogs with spirocyclohexyl and spirofluorenyl groups at C(10) are reported. Conformation-determining torsion angles and key hydrogen bond distances and angles are compared to those from molecular dynamics calculations, and to the corresponding data from X-ray determinations and molecular dynamics calculations of bilirubin. Like bilirubin, the component dipyrrinones of spirocyclohexyl and spirofluorenyl rubins are present in the bis-lactam form with (*Z*)-configuration double bonds at C(4) and C(15). Their crystal structures show considerable similarity to that of bilirubin: both pigments adopt a folded, intramolecularly hydrogen-bonded ridge-tile conformation stabilized by six hydrogen bonds. The interplanar angle of the spirocyclohexyl ridge-tile is nearly the same (94°) as that of bilirubin (∼95°), but the interplanar angle of the spirofluorenyl ridge-tile is noticeably smaller (84°). The hydrogen bond distances of both spirorubin crystal structures are generally longer by 0.1–0.2 Å than those in bilirubin. Both new pigments exhibit excellent lipophilicity and, unlike bilirubin, are soluble in methanol.

Keywords. Linear tetrapyrroles; Stereochemistry, Hydrogen bonding.

Introduction

The bile pigment of mammals, bilirubin (Fig. 1A), is an important and conformationally interesting member of the linear tetrapyrrole class [1] and the yellow pigment of jaundice [2, 3]. Composed of two dipyrrinones conjoined to a CH_2 group (Fig. 1B), bilirubin is flexible about the center, and it is the relative orientation of these dipyrrinones about C(10) that determines the shape of the pigment. The most stable stereochemistry is not linear (Fig. 1A), but one where the dipyrrinones are rotated into a conformation shaped like a half-opened book (Fig. 1B) or ridge-tile, and in which intramolecular nonbonded steric interactions are minimized and the structure is greatly stabilized by a matrix of six intramolecular

* Corresponding author. E-mail: lightner@scs.unr.edu

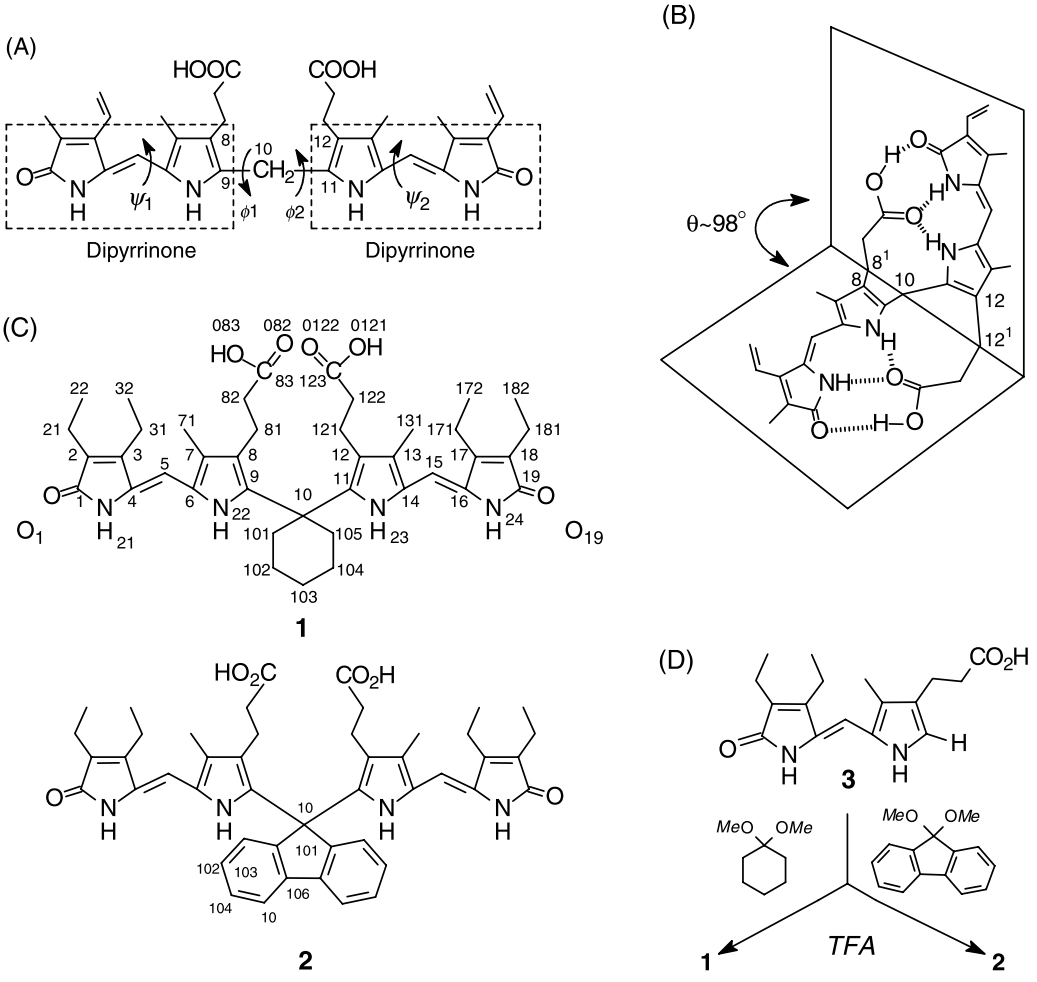

Fig. 1. (A) Bilirubin in a high-energy linear conformational representation with angles of rotation about the C(9)–C(10) and C(10)–C(11) bonds, ϕ_1 and ϕ_2, $\sim$180°; rotations of the dipyrrinones about torsion angles ϕ_1 and ϕ_2 interconvert the ridge-tile and linear conformations, as well as others (porphyrin-like); rotations about ψ_1 and ψ_2 within the two dipyrrinones distort the chromophores from planarity; (B) In the energy-minimized conformation shaped like a ridge-tile with $\phi_1 = \phi_2 \sim 60°$ and an interplanar angle of $\sim$98°; the ridge-tile seam lies approximately along the line connecting carbons 8^1, 10, and 12^1; in the ridge-tile, the dipyrrinones are planar, $\psi_1 \sim \psi_2 \sim 0°$; this conformation achieves considerable stabilization from intramolecular hydrogen bonds (hatched lines); (C) The spirocyclohexyl (**1**) and spirofluorenyl (**2**) rubins of this work with the numbering of atoms from the X-ray crystal structures; (D) The dipyrrinone precursor (**3**) to spiro-rubins **1** and **2**

hydrogen bonds [4]. Dipyrrinones are known to be avid participants in hydrogen bonding, capable of strong self-association to form hydrogen-bonded dimers [5, 6], and an even stronger attraction to engage carboxylic acids in hydrogen bonding [7, 8]. Thus, each dipyrrinone of bilirubin clings to a carboxylic acid, thereby adding considerable additional stabilization to the ridge-tile conformation [4], which is the only conformation of bilirubin observed in crystals [9] of bilirubin by X-ray crystallography and by solid state NMR [10]. Solution NMR studies [10, 12] and circular dichroism spectroscopy [4, 13] confirm its dominance in solution, even when the

carboxyl groups are ionized, and molecular mechanics energy calculations [4] support the general notion that this conformation is very strongly stabilized.

Very few crystal structures have been obtained for bilirubins [1, 9, 14–17], which is due largely to the considerable difficulty encountered in growing suitable crystals. The crystal structure of a 10-substituted bilirubin, 10-isopropyl-3,17-bisnor-mesobilirubin-XIIIα showed that the presence of the isopropyl group caused the dihedral angle (θ of Fig. 1B) to open slightly while maintaining full intramolecular hydrogen bonding [16]. Our continued interest in bilirubin stereochemistry and its stabilization by intramolecular hydrogen bonds between propionic acid and dipyrrinone groups led us to consider whether such hydrogen bonding might be retained in a bilirubin analog with both small and large spirocyclic groups at C(10), the sensitive ''hinge'' of the ridge-tile. Earlier solution studies of 10,10-dimethyl bilirubin analogs [18] indicated that the *gem*-dimethyl group did not interfere with intramolecular hydrogen bonding and also enhanced solubility in organic solvents. In order to probe further the 10,10-dialkyl effect, we prepared two new bilirubin analogs, one with a spirocyclohexyl (**1**) and a second with a larger spirofluorenyl group (**2**, Fig. 1C).

In the present communication, we describe stereochemical investigations of **1** and **2** based on their X-ray crystal structures and molecular mechanics calculations. These results are compared to bilirubin X-ray crystal determinations [9a, 9b, 14, 15] and molecular dynamics calculations [1, 4, 13].

Results and Discussion

Synthesis and Spectra

Using synthetic methodology developed earlier [17a], the known 9-*H* dipyrrinone (**3**, Fig. 1D) [18a] was reacted smoothly at 0°C in the presence of trifluoroacetic acid with 1,1-dimethoxycyclohexane [19] to give **1**, or 9,9-dimethoxyfluorene [19] to give **2**. The isolated yields of pure compounds were 44 and 49%.

The structures of **1** and **2** follow from the method of synthesis and the starting materials and were confirmed by ^{13}C NMR spectroscopy by comparison with the known 2,18-diethylmesobilirubin-XIIIα (**4**) [18a] (Table 1). In addition to the close match of the carbons of the rubin core, new signals for cyclohexyl carbons in **1** and fluorenyl carbons in **2** are seen, and the expected deshieldings due to *gem*-substitution at C(10) are observed at C(10), which is a singlet in **1** and **2**, and at nearby C(9,11). In addition, C(8^2,12^2) of the propionic acid chains of **2** are more shielded than in **1** or the parent rubin, suggesting a close proximity to the face of the aromatic rings of the fluorene.

The structures of **1** and **2**, including their 4*Z*,15*Z* stereochemistry are supported by N*O*E measurements in $CDCl_3$ (Fig. 2), which also shows a weak N*O*E between the carboxylic acid and lactam hydrogens. The latter indicate a close proximity between these functional groups, as might be found in an intramolecularly hydrogen-bonded conformation, *e.g.*, as in Fig. 1B. Additional support for intramolecular hydrogen bonding may be found in the carboxylic acid lactam and pyrrole NH chemical shifts (Table 2). In $CDCl_3$ solvent: (i) the lactam NHs are characteristically more deshielded than the pyrrole NHs, which typically lie at $\sim$9 ppm – or $\sim$1 ppm higher field than found in $(CD_3)_2SO$ solvent and (ii) the CO_2H resonance is typically more deshielded than in $(CD_3)_2SO$ [8, 11a, 12a, 20a, 21].

Table 1. Comparison of ^{13}C NMR chemical shifts[a] and assignments of 10,10-spirocyclohexyl rubin **1**, 10,10-spirofluorenyl rubin **2** and their parent, 2,18-diethylmesobilirubin-XIIIα (**4**)

Carbon[b]	δ, $(CD_3)_2SO$			δ, $CDCl_3$		
	1	**2**	**4**	**1**	**2**	**4**
1, 19	172.1	172.4	171.5	174.7	175.0	174.7
2, 18	128.4	128.7	128.7	127.2	128.2	128.5
2^1, 18^1	16.37	16.35	16.20	16.66	16.70	16.69
2^2, 18^2	13.90	13.80	13.60	13.92	13.96	13.77
3, 17	146.9	148.5	146.7	147.9	148.1	147.9
3^1, 17^1	17.05	17.05	16.85	17.63	17.66	17.71
3^2, 17^2	15.74	15.76	15.46	15.90	15.81	15.70
4, 16	129.2	127.8	127.8	129.0	128.8	129.4
5, 15	98.52	97.73	97.80	100.8	100.4	100.6
6, 14	123.2	123.3	122.3	124.2	124.2	123.6
7, 13	122.0	123.2	122.0	125.7	125.1	124.6
7^1, 13^1	9.33	9.23	9.00	10.97	10.47	10.03
8, 12	119.0	118.9	119.2	119.0	119.3	119.5
8^1, 12^1	19.85	19.54	19.20	20.63	18.05	18.63
8^2, 12^2	33.7	33.60	34.35	32.87	31.26	32.72
8^3, 12^3	174.0	173.5	173.8	180.5	179.0	179.5
9, 11	137.3	131.7	130.1	139.8	135.4	133.2
10	40.78	56.91	25.00	46.97	59.81	29.70
10^1	35.46	39.9	–	38.16	139.8	–
10^2	25.31	129.4	–	26.25	128.0	–
10^3	22.97	127.7	–	23.66	128.8	–
10^4	–	125.8	–	–	126.9	–
10^5	–	120.1	–	–	119.7	–
10^6	–	146.8	–	–	145.5	–

[a] δ (ppm) downfield from $(CH_3)_4Si$; [b] see Fig. 1C for numbering system used

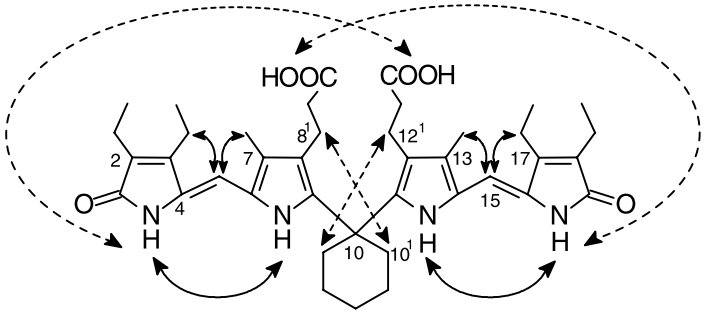

Fig. 2. N*O*Es found for 10,10-spirocyclohexyl rubin **1** in $CDCl_3$ are shown by curved, double-headed arrows; weak N*O*Es are shown by curved, dashed arrows; the same N*O*Es are found in the 10,10-spirofluorenyl analog **2**, except N*O*Es are not seen between C(8^1,12^1) and the hydrogens of the fluorene component, and they were too weak to be detected between the lactam NH and propionic acid COOH hydrogens

Table 2. Comparison of NH and COOH chemical shifts[a] of 10,10-spirocyclohexyl rubin **1**, 10,10-spirofluorenyl rubin **2**, and 2,18-diethylmesobilirubin-XIIIα (**4**) in $CDCl_3$ and *DMSO*-d_6

Pigment	δ, $CDCl_3$			δ, $(CD_3)_2SO$		
	Pyr-NH	*Lac*-NH	–COOH	*Pyr*-NH	*Lac*-NH	–COOH
1	9.10	11.40	14.31	10.07	9.56	11.86
2	9.50	11.50	13.30	10.47	10.24	11.89
4	9.14	10.59	13.67	10.32	9.78	11.9

[a] δ (ppm) downfield from $(CH_3)_4Si$

Table 3. Chemical shifts and assignments for the ABCX multiplets of the $-CH_AH_XCH_BH_C-COOH$ of 10,10-spirocyclohexyl rubin **1**, 10,10-spirofluorenyl rubin **2**, and their parent, 2,18-diethylmesobilirubin-XIIIα (**4**) in $CDCl_3$

Pigment	H_A	H_B	H_C	H_X
1[a]	3.52	2.64	2.80	2.64
2[b]	3.50	2.93	2.78	2.55
4[c]	2.99	2.89	2.78	2.54

[a] $J_{AB} = 11.90$ Hz, $J_{AC} = 2.2$ Hz, $J_{AX} = -13.20$ Hz, $J_{BC} = -18.60$ Hz, $J_{BX} = 2.8$ Hz, $J_{CX} = 4.8$ Hz;
[b] $J_{AB} = 12.60$ Hz, $J_{AC} = 2.50$ Hz, $J_{AX} = -14.50$ Hz, $J_{BC} = -18.60$ Hz, $J_{BX} = 2.60$ Hz, $J_{CX} = 3.90$ Hz;
[c] $J_{AB} = 13.80$ Hz, $J_{AC} = 2.60$ Hz, $J_{AX} = -15.40$ Hz, $J_{BC} = -18.80$ Hz, $J_{BX} = 3.00$ Hz, $J_{CX} = 4.60$ Hz

Further evidence for intramolecular hydrogen bonding between propionic acid and dipyrrinone groups in the mesobilirubins can be elicited from an examination of vicinal coupling constants. In $CDCl_3$ solvent, the well-defined ABCX (ddd) coupling pattern is characteristic of restricted mobility [11a, 12a, 12d, 21] in the $-CH_AH_XCH_BH_C-COOH$ segment which is constrained to adopt a fixed staggered geometry (Table 3) due to strong intramolecular hydrogen bonding. Analysis of the vicinal H–H coupling constants in the propionic acid chains (Table 3) clearly shows the ABCX pattern of the fixed staggered propionic acid geometry in **1** and **2** (as well as **4**), thus providing strong supporting experimental evidence for folded ridge-tile structures. On the other hand, a less complicated A_2B_2 pattern is found in $(CD_3)_2SO$ solvent, indicating more motional freedom in the propionic acid segment, whose CO_2H groups are thought to be linked to the dipyrrinones *via* bound solvent molecules [12a, 12b, 22].

Crystal Structure and Conformation

An examination of the crystal structure drawings of the X-ray structures of **1** and **2** clearly indicates that the molecules are folded into a ridge-tile conformation (Fig. 3), a conformation consistent with that found in crystals of bilirubin [11a, 11b, 14], mesobilirubin-IXα [11d], bilirubin-IXα bisisopropyl ammonium salt [15], and 10-isopropylglaucorubin [16]. The seam of the ridge-tile lies approximately along the line connecting C(81), C(10), and C(121) (Fig. 1B) (or C(81)–C(10)–C(121) of **1** or **2** in Fig. 3), where the two planes containing the two dipyrrinones intersect at an interplanar angle (θ) of about 94° in **1** and 84° in **2** (Table 4). Thus, in **1** θ is

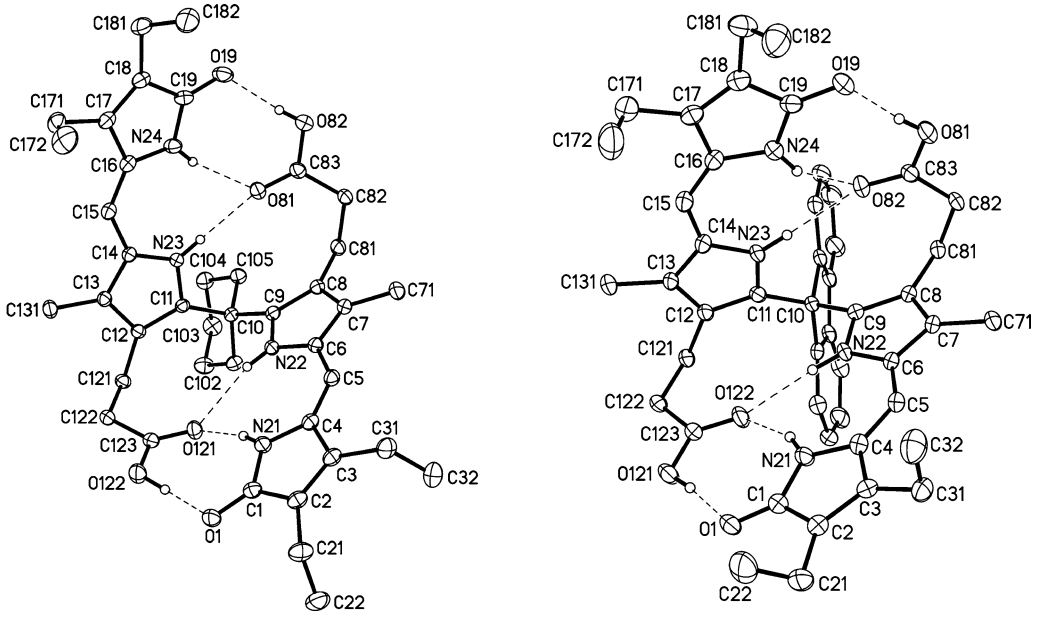

Fig. 3. Crystal structure drawings and numbering system of **1** and **2**; hydrogen atoms are removed for clarity of presentation; librational ellipsoids have been drawn with 50% probability

Table 4. Comparison of conformation-determining torsion angles (°) from X-ray crystallography and molecular dynamics (MD)[a] calculations for cyclohexyl rubin **1**, fluorenyl rubin **2**, and bilirubin (**BR**)

Structure/Method		ϕ_1(11-10-9-22)[c]	ϕ_2(9-10-11-23)[c]	ψ_1(4-5-6-22)[d]	ψ_2(16-15-14-23)[c]
1	X-ray	−60	−64	−4.6	−8.6
	MD	−60	−60	15	5
2	X-ray	−53	−53	−5.7	−0.4
	MD	60	60	−8.7	−7.9
BR[b]	X-ray	60	64	18	−2.7
	MD	59	58	16	16
Structure/Method		(N21-4-5-6)[e]	(14-15-16-24)[e]	θ(dipyrrinone)[f]	θ(pyrrole)[f]
1	X-ray	+2.4	−4.5	94	95
	MD	1.0	1.0	94	91
2	X-ray	−1.3	−1.2	84	84
	MD	−0.9	−0.8	92	92
BR[b]	X-ray	11	5.8	95	99
	MD	1.0	−0.2	88	94

[a] Using Sybyl ver. 6.9 for the SGI workstation, Ref. [25]; [b] data taken from X-ray diffraction coordinates given in Ref. [9a]; [c] values would be ∼0° for the prophyrin conformation, ∼60° for the ridge-tile conformation, and ∼180° for the linear conformation; [d] indicates distortion from a planar dipyrrinone, where $\psi \sim 0°$; [e] indicates twist from 0° of C=C; [f] interplanar dihedral angle using the average plane of each dipyrrinone or the dihedral angle of the two pyrroles adjacent to C(10)

Table 5. Comparison of hydrogen bond distances (*d*) and angles (°) from X-ray crystallography and molecular dynamics (MD) calculations[a] for lactam (*L*) NH, pyrrole (*P*) NH, and acid (OH) for 10,10-spirocyclohexyl rubin **1**, 10,10-spirofluorenyl rubin **2**, and bilirubin (**BR**)

Method		Hydrogen bond distances			Hydrogen bond angles		
		*L*N–H···O	*P*N–H···O	O–H···O	*L*N–H···O	*P*N–H···O	O–H···O
1	X-ray	1.98	2.20	1.67	154	162	175
		1.88	2.06	1.87	167	172	169
	MD	1.50	1.73	1.53	156	161	172
		1.50	1.80	1.53	166	167	172
2	X-ray	1.87	2.11	1.80	159	166	173
		1.90	2.14	1.77	157	166	173
	MD	1.51	1.70	1.54	162	170	171
		1.51	1.70	1.54	163	171	171
BR[b]	X-ray	1.8	1.8	1.5	160	157	180
					162	157	186
	MD	1.6	1.6	1.5	153	164	169
					152	165	169

[a] Using Sybyl vers. 6.9 for the SGI workstation, Ref. [25]; [b] data taken from X-ray diffraction coordinates given in Ref. [9a]

essentially the same as that ($\theta \sim 95°$) found in crystals of bilirubin [9a, 9b], but in **2** it is smaller – possibly due to the constraints of the 5-membered ring. Apparently the *gem*-dialkyl substitution *per se* does little to open up or close down the pitch of the ridge-tile. The pyrrole and lactam nitrogens of **1** and **2** lie in close proximity to the propionic carboxyl oxygens, making hydrogen bonding possible and likely. The calculated carboxylic acid oxygen to pyrrole/lactam hydrogens have an average hydrogen bond distance of about 1.9–2.2 Å (Table 5), which is longer than that found in the X-ray structure of bilirubin (−1.8 Å), in the X-ray structure [9a, 9b]. The lactam oxygen to carboxylic acid hydrogen bond is also longer (1.7–1.8 Å) in **1** and **2** as compared to that of bilirubin (1.5 Å). These data suggest that the propionic acids of **1** and **2** are less tightly hydrogen bonded to their opposing dipyrrinones than in bilirubin.

The crystal structure conformation of **1** and **2** correlates qualitatively well with that predicted from solution NMR studies. The dipyrrinones adopt a (*syn-Z*) configuration of the C=C at C(4) and C(15). The observed bond lengths suggest that delocalization over an individual conjugated system of two pyrrole rings is rather limited, since C(4)=C(5) and C(15)=C(16) double bonds seem to be essentially full double bonds (average bond length of 1.35 Å). The same bond lengths are found in the crystal structure of 10-isopropylglaucorubin [16]; however, they are slightly longer than in bilirubin (average bond length of 1.30 Å). As suggested earlier for bilirubin [9a, 9b], mesobilirubin [9c], and its isopropyl analog [16], spiro-rubins **1** and **2** can be regarded as 2,2′-dipyrrylmethanes with conjugating substituents at the α positions.

It has been demonstrated that when the possibility of lactam/lactim tautomerism exists, the lactam form predominates [23] by about 4–10 orders of magnitude over the lactim form for bile pigments in solution [9c] and in all known rubin X-ray structures [9, 14–17, 23]. Consistent with this, spiro-rubins **1** and **2** are found to prefer the bis-lactam tautomeric form, as confirmed by lactam C=O bond lengths that are comparable to C=O distances in ordinary lactams. The C(1)=O(1) and C(19)=O(19) bond lengths of **1** are 1.26, 1.25 Å, which compare favorably with those of 10-isopropylglaucorubin (1.25, 1.26 Å) [16], a 10-thiarubin (1.25 Å) [17], and bilirubin [9a, 9b, 14] where the corresponding bond lengths are 1.25 and 1.28 Å. Furthermore, the lactam C–N bond distances in **1** and **2** are consistent with a carbon nitrogen *single* bond, C(1)–N(21) ~ 1.35 Å, C(19)–N(24) ~ 1.35–1.36 Å – identical to those of 10-isopropylglaucorubin [16] and very similar to those found in bilirubin [9a, 9b, 9c] (1.41 and 1.35 Å). In contrast, for the lactim (methyl ether) structure, as in 5-ethoxy-5′-ethoxycarbonyl-3′,4′-dihydro-3,4-dimethyl-2,2′-pyrromethane [24], the C=N and C–O(Et) bond distances are 1.28 and 1.33 Å. For bilirubin, the lactam tautomer was proven independently by ^{15}N NMR: $\delta_{N(21)} = -249.8$, $\delta_{N(24)} = -249.2$, $\delta_{N(22)} = -231.3$, $\delta_{N(23)} = -231.6$ *vs.* $\delta_N = -140$ ppm for a lactim N [1].

Comparison of Conformation from Molecular Dynamics Calculations and X-Ray Analysis

Insight into the preferred conformation of bilirubin and its 10,10-spiro analogs may also be obtained from molecular dynamics computations using the Tripos Sybyl force field [25]. Torsion angles (C–C) about the carbon-carbon bonds linking the four rings are largely responsible for determining the pigment's conformation and helicity. Such torsion angles and helical pitch can be extracted from atomic coordinates of the minimum energy conformation determined by molecular dynamics calculations [1, 4] and compared to those determined by X-ray crystallography [1, 9]. Comparison of the relevant torsion angles obtained from both techniques for **1**, **2**, and bilirubin is shown in Table 4.

Significantly, molecular dynamics calculations [25], which do not take into account crystal packing forces, reproduce the experimental data rather well, predicting nearly the same torsion angles (ϕ_1 and ϕ_2) about C(9)–C(10) and C(10)–C(11) for **1** and for bilirubin and slightly smaller dihedral angles (θ) between the two dipyrrinone average planes (Table 4). However, the computed ϕ_1, ϕ_2, and θ angles of **2** are noticeably larger than those from the crystal structure, by 7–8°. Nonetheless, it can be seen from these parameters that the global minimum energy conformations of **1**, **2**, and bilirubin are very similar, with the ridge-tile of **2** being somewhat more closed (steeper pitch) than that in **1** or bilirubin. A ridge-tile adapted to a roof of much steeper pitch was also found in the crystal of 2,18-diethyl-10-thiamesobilirubin-XIIIα ($\theta = 86°$) [17], which we attribute to the small C–S–C bond angle. In **2**, the small dihedral angle ($\theta = 84°$) is probably related to the presence of the spiro 5-ring. Within the dipyrrinones there is less distortion from planarity in **1** and **2** than in bilirubin (*cf.* ψ_1 and ψ_2 of Table 5). In the dipyrrinone component of **1** and **2** the slight distortion from planarity appears to come mainly from twisting of the C(5)–C(6) and C(14)–C(15) single bonds, as

there is very little distortion or twist in the C(4)=C(5) and C(15)=C(16) double bonds. In bilirubin, there is more twist in both of the corresponding single and double bonds and presumably slightly less effective π-conjugation within a given dipyrrinone unit. Somewhat greater π-delocalization or conjugation in **1** and **2**

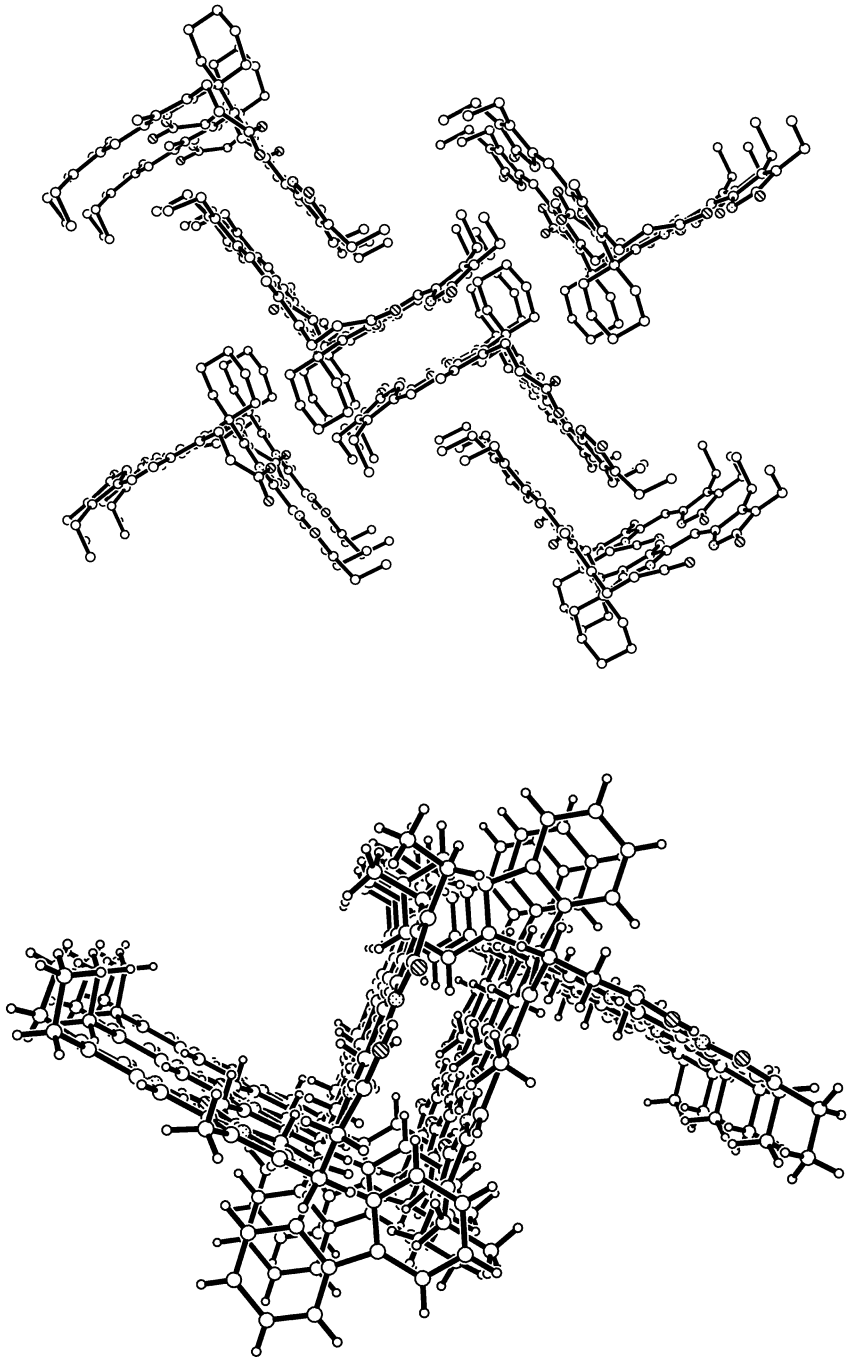

Fig. 4. Molecular packing of spiro-rubins **1** (upper) and **2** (lower) in projections showing their ridge-tile conformation

relative to bilirubin may be assumed from the slightly longer C(4)=C(5) and C(15)=C(16) bond lengths found in the X-ray structure, averaging ~1.35 Å, compared to bilirubin where the corresponding average bond length is (~1.30 Å), indicating more delocalization in the former relative to the latter.

A comparison of hydrogen bond distances and hydrogen bond angles in **1** and bilirubin from their crystal structures and their global minimum energy structures determined by molecular dynamics calculations is given in Table 5. The hydrogen bond distances are appreciably longer in crystalline **1** and **2** than in the computed energy-minimized structures, much smaller differences were observed in bilirubin. Apparently not caused by significant distortions of the ridge-tile in the crystal, the N–H · · · O=C hydrogen bonds are extended by ~20%, and the O–H · · · O=C hydrogen bond to lengthen by ~30% – all relative to the computed energy-minimum structure. Yet, all computed and ''observed'' (X-ray) hydrogen bond angles of **1** and **2** lie within a few percent of each other and with 25° of the optimum angle of 180°.

Crystal Packing

The stacking pattern in **1** and **2** (Fig. 4) is very similar to that found in bilirubin and mesobilirubin [9]. The ridge-tiles are stacked with their dipyrrinone systems parallel to one another (at the *van der Waals* distance), thereby giving rise to channels in the crystal lattice in which disordered CH_2Cl_2 or $CHCl_3$ solvent molecules reside. Stacks of ridge-tile shaped molecules of **1** and **2** interleave with similar but inverted stacks. There is little evidence of *intermolecular* association as the hydrogen bond pattern is almost exclusively *intramolecular*. The stacking pattern described here is very characteristic of intramolecularly hydrogen-bonded ridge-tile conformers of bilirubins [10, 15] but it is very different than the stacking pattern of those bilirubins which cannot or do not attain ridge-tile conformations in the solid state [14, 24].

Experimental

NMR spectra were obtained in $CDCl_3$ solvent on a GE QE-300 spectrometer operating at 300 MHz (unless otherwise indicated), or on a Varian Unity Plus 500 MHz spectrometer. HMQC, HMBC, and N*O*E NMR were obtained on a 500 MHz spectrometer. Chemical shifts are reported in δ (ppm) referenced to the residual $CHCl_3$ ^1H signal at 7.26 ppm and ^{13}C at 77.23 ppm. Infrared spectra were recorded on a Perkin-Elmer model 1610-FT IR instrument. Ultraviolet-visible spectra were recorded on a Perkin-Elmer λ-12 spectrophotometer, GC-MS analyses were carried out on a Hewlett-Packard GC-MS Model 5890A ion selective detector equipped with a DB-1 (100% dimethylpolysiloxane) column. Melting points were taken on a Mel-Temp capillary apparatus. Combustion analyses were carried out by Desert Analytics, Tucson, AZ and gave agreement within ±0.3% of theoretical. Analytical thin layer chromatography (TLC) was carried out on J.T. Baker silica gel IB-F plates (125 µm layers). Flash column chromatography was carried out using silica gel, 60–200 mesh (M. Woelm). Radial chromatography was carried out on Merck preparative layer grade silica gel PF_{254} with $CaSO_4$ binder using a Chromatotron (Harrison Research, Inc., Palo Alto, CA) with 1, 2, or 4 mm thick rotors. Commercial reagents were used as received from Aldrich or Acros; HPLC grade CH_3OH was from Fisher. Spectroscopic data were obtained in spectral grade solvents from Fisher and Acros. $CDCl_3$ and *DMSO*-d_6 were from Cambridge Isotope Laboratories. Dipyrrinone **3** was available from previous work [18a].

10,10-Spiro[cyclohexyl]-2,18-bishomomesobilirubin-XIIIα (**1**, $C_{40}H_{52}N_4O_6$)

To cold (0°C) *TFA* (2.2 cm^3) was added 2,18-diethylneoxanthobilirubic acid (**3**, 200 mg, 0.66 mmol) soaked with 1,1-dimethoxycyclohexane (97 mm^3, 0.64 mmol, 0.97 equiv) under vigorous stirring. After 5 min, 50 cm^3 of ice-cold H_2O were added to the reaction mixture. The dirty green precipitate was collected by filtration, washed with water, and dried *in vacuo*. The collected precipitate was washed with liberal amounts of dichloromethane, and the yellow-green solutions of CH_2Cl_2 were combined and saved. The residue that did not dissolve was mainly starting material, and was treated with 1,1-dimethoxy propane (47 mm^3) and cold (0°) *TFA* (1.1 mm^3) for 5 min, followed by the same treatment as above. The procedure was repeated once more, and the combined dichloromethane washings were concentrated on a rotovap. The yellow-green solid material thus obtained was radially chromatographed ($CHCl_3$:*Et*OH = 95:5 by vol) yielding **1** as a pure yellow-orange product. Yield 100 mg (44% after 3 cycles); mp 248°C (dec); IR (deposition from CH_2Cl_2): $\bar{\nu} = 3440$, 2965, 1705, 1690, 1675, 1610, 1590 cm^{-1}; ^{1}H NMR ($CDCl_3$, 500 MHz): $\delta = 1.08$ (t, $J = 7.5$ Hz, 6H), 1.15 (t, $J = 7.5$ Hz, 6H), 1.33–1.73 (m, 10H), 2.15 (s, 6H), 2.31 (q, $J = 7.3$ Hz, 4H), 2.50 (q, $J = 7.3$ Hz, 4H), 2.63–3.52 (m, ABCX, 4H), 6.06 (s, 2H), 9.11 (brs, 2H, NH), 11.40 (brs, 2H, NH), 14.31 (brs, 2H, COOH) ppm; ^{13}C NMR in Table 1.

10,10-Spiro[fluorenyl]-2,18-bishomomesobilirubin-XIIIα (**2**, $C_{47}H_{50}N_4O_6$)

This compound was prepared by the acid catalyzed condensation reaction of 2,18-diethyl-neoxanthobilirubic acid (**3**, 200 mg, 0.66 mmol) and 9,9-dimethoxyfluorene (145 mg, 0.64 mmol, 0.97 equiv) following the same procedure as above. Purification was achieved using radial chromatography, which gave **2** as a yellow solid. Yield 125 mg (49% after 2 cycles); mp 250°C (dec); ^{1}H NMR ($CDCl_3$, 500 MHz): $\delta = 1.12$ (t, $J = 7.5$ Hz, 6H), 1.20 (t, $J = 7.5$ Hz, 6H), 2.03 (s, 6H), 2.40 (q, $J = 7.6$ Hz, 4H), 2.54 (q, $J = 7.6$ Hz, 4H), 6.07 (s, 2H), 7.26 (t, $J = 3.8$ Hz, 2H), 7.37 (t, $J = 3.8$ Hz, 2H), 7.74 (d, $J = 3.88$ Hz, 2H), 8.24 (d, $J = 3.88$ Hz, 2H), 9.50 (brs, 2H, NH), 11.50 (brs, 2H, NH), 13.30 (brs, 2H, COOH) ppm; ^{13}C NMR in Table 1.

X-Ray Structure and Solution

Crystals of spirocyclohexyl rubin **1** were grown by slow diffusion of *n*-hexane into a solution of $CHCl_3$. A crystal (approximate dimensions $0.53 \times 0.61 \times 0.116$ mm^3) was placed onto the tip of a 0.1 mm diameter glass capillary and mounted on a Bruker SMART Apex system for data collection at 100(2) K. Similarly, a crystal of **2**, grown from CH_2Cl_2/*n*-hexane and of approximate dimensions $0.48 \times 0.30 \times 0.14$ mm^3 was mounted and analyzed. A preliminary set of cell constants was calculated from reflections harvested from 3 sets of 20 frames. These initial sets of frames were oriented such that orthogonal wedges of reciprocal space were surveyed (final orientation matrices determined from global least-squares refinement of 6379 reflections for **1** and 7071 reflections for **2**). The data collection was carried out using MoKα radiation (0.71073 Å graphite monochromator) with a frame time of 10 sec and a detector distance of 4.94 cm. A randomly oriented region of reciprocal space was surveyed to the extent of 2 hemispheres and to a resolution of 0.68 Å. Four major sections of frames were collected with 0.3° steps in ω at 600 different ϕ settings and a detector position of 36° in 2θ. The intensity data were corrected for absorption and decay (SADABS) [26]. Final cell constants were calculated from the *xyz* centroids of strong reflections from the actual data collection after integration (SAINT 6.01, 1999) [27]. Crystal data and refinement information for **1** and **2** may be found in Table 6.

The structure was solved using SHELXS-93 [27] and refined using SHELXL-97 [28]. The triclinic space group *PT* was determined based on systematic absences and intensity statistics. A direct-methods solution was calculated which provided most non-hydrogen atoms from the E-map. Full-matrix least squares/difference *Fourier* cycles were performed which located the remaining non-hydrogen

Table 6. Crystal data and structure refinement for 10,10-spirocyclohexyl rubin **1** and 10,10-spirofluorenyl rubin **2**

	1 • $CHCl_3$	**2 • 0.75 CH_2Cl_2**
Formula weight	648.88	766.94
Crystallized from	$CHCl_3$/*n*-hexane	CH_2Cl_2/*n*-hexane
Temperature/K	123(2)	100(2)
Formula	$C_{41}H_{53}Cl_3N_4O_6$	$C_{47.75}H_{50}Cl_{1.5}N_4O_6$
Crystal size/mm^3	$0.53 \times 0.161 \times 0.116$	$0.48 \times 0.30 \times 0.14$
Crystal system	Triclinic	Triclinic
Space group	*P*-1	*P*-1
Z	2	2
Unit cell dimensions	$a = 11.9410(8)$ Å $\alpha = 72.115(3)^\circ$	$a = 11.9122(14)$ Å $\alpha = 68.893(2)^\circ$
	$b = 12.6516(8)$ Å $\beta = 68.157(4)^\circ$	$b = 15.0395(18)$ Å $\beta = 78.728(2)^\circ$
	$c = 15.1467(12)$ Å $\gamma = 84.927(4)^\circ$	$c = 15.6109(19)$ Å $\gamma = 70.343(2)^\circ$
Volume/$Å^3$	2020.5(2)	2448.3(5)
Density (calculated)/$Mg\,m^{-3}$	1.322	1.125
Absorption coefficient/mm^{-1}	0.278	0.153
F(000)	852	876
Crystal habit and color	Plate, Yellow	Plate, Yellow
Theta range for data collection/°	1.52 to 30.00	1.4 to 25.00
Index ranges	$-16 \le h \le 16$, $-17 \le k \le 17$, $-21 \le l \le 20$	$-14 \le h \le 14$, $-17 \le k \le 17$, $-18 \le l \le 18$
Reflections collected	26032	18810
Independent reflections	11297 [R(int) = 0.0197]	8486 [R(int) = 0.0427]
Observed reflections	9564	5917
Completeness to theta/%	95.6	98.5
Absorption correction	SADABS	SADABS
Max. and min. transmission	1.00 and 0.759	0.979 and 0.931
Refinement method	Full-matrix least-squares on F^2	Full-matrix least-squares on F^2
Data/restraints/parameters	11297/0/699	848/15/587
Goodness-of-fit on F^2	1.083	1.061
Final R indices [$I > 2\sigma(I)$]	$R1 = 0.0513$, $wR2 = 0.1428$	$R1 = 0.0879$, $wR2 = 0.2608$
R indices (all data)	$R1 = 0.0593$, $wR2 = 0.1490$	$R1 = 0.1137$, $wR2 = 0.2801$
Largest diff. peak and hole/e$Å^{-3}$	1.175 and −1.132	1.518 and −0.467

atoms. All non-hydrogen atoms were refined with anisotropic displacement parameters unless stated otherwise. The data were corrected for absorption using an empirical model derived from psi scans. Hydrogen atom positions were placed in ideal positions and refined as riding atoms with relative isotropic displacement parameters (a C–H distance fixed at 0.96 Å and a thermal parameter 1.2 times the host carbon atom). Tables of atomic coordinates, bond lengths and angles, anisotropic displacement parameters, hydrogen coordinates, and isotropic displacement parameters have been deposited at the Cambridge Crystallographic Data Centre, CCDC No. 227589 for **1** and CCDC No. 227590 for **2**.

Acknowledgements

We thank the U.S. National Institutes of Health (HD-17779) for generous support of this work. We also thank the National Science Foundation (CHE-0226402) for providing funding to purchase the X-ray diffractometer used in this work.

References

[1] Falk H (1989) The Chemistry of Linear Oligopyrroles and Bile Pigments. Springer, Wien
[2] McDonagh AF (1979) Bile Pigments: Bilatrienes and 5,15-Biladienes. In: Dolphin D (ed) The Porphyrins, vol 6. Academic Press, New York, p 293
[3] Chowdhury JR, Wolkoff AW, Chowdhury NR, Arias IM (1979) Hereditary Jaundice and Disorders of Bilirubin Metabolism. In: Scriver CR, Beaudet AL, Sly WS, Valle D (eds) The Metabolic and Molecular Basis of Inherited Disease, vol II. McGraw-Hill, New York, pp 2161–2208
[4] Person RV, Peterson BR, Lightner DA (1994) J Am Chem Soc **116**: 42
[5] Huggins MT, Lightner DA (2001) Monatsh Chem **132**: 203
[6] Nogales DF, Ma JS, Lightner DA (1993) Tetrahedron **49**: 2361
[7] Boiadjiev SE, Anstine DT, Lightner DA (1994) Tetrahedron Asymm **5**: 1945
[8] Huggins MT, Lightner DA (2001) Tetrahedron **57**: 2279
[9] a) Bonnett R, Davies JE, Hursthouse MB, Sheldrick GM (1978) Proc R Soc London Ser B **202**: 249; b) LeBas G, Allegret A, Mauguen Y, DeRango C, Bailly M (1980) Acta Crystallogr Sect B **B36**: 3007; c) Becker W, Sheldrick WS (1978) Acta Crystallogr Sect B **B34**: 1298
[10] Brown SP, Zhu XX, Saalwächter K, Spiess HW (2001) J Am Chem Soc **123**: 4275
[11] a) Kaplan D, Navon G (1983) Israel J Chem **23**: 177; b) Kaplan D, Navon G (1983) Org Magn Res 198; c) Kaplan D, Navon G (1982) Biochem J **201**: 605; d) Navon G, Frank S, Kaplan D (1984) J Chem Soc Perkin Trans 2, 1145
[12] a) Doerner T, Knipp B, Lightner DA (1997) Tetrahedron **53**: 2697; b) Nogales D, Lightner DA (1995) J Biol Chem **270**: 73
[13] Boiadjiev SE, Person RV, Puzicha G, Knobler C, Maverick E, Trueblood KN, Lightner DA (1992) J Am Chem Soc **114**: 10123
[14] For a review of crystal structures of linear polypyrrolic compounds, see Sheldrick WS (1983) Israel J Chem **23**: 155
[15] Mugnoli A, Manitto D, Monti D (1983) Acta Crystallogr Sect C **39**: 287
[16] Kar AK, Tipton AK, Lightner DA (1999) Monatsh Chem **130**: 833
[17] Tipton A, Lightner DA (2002) Monatsh Chem **133**: 707
[18] a) Xie M, Lightner DA (1993) Tetrahedron **49**: 2185; b) Xie M, Holmes DL, Lightner DA (1993) Tetrahedron **49**: 9235
[19] a) Taylor EC, Chiang C-S (1977) Synthesis 467; b) Bakthayachalam V, Lin LG, Chenan XM, Czarnik AW (1987) Carbohydrate Research **170**: 124
[20] a) Huggins MT, Lightner DA (2000) J Org Chem **65**: 6001; b) Huggins MT, Lightner DA (2000) Tetrahedron **56**: 1797
[21] a) Brower JO, Lightner DA, McDonagh AF (2000) Tetrahedron **56**: 7869; b) Boiadjiev SE, Lightner DA (1999) Tetrahedron Asymm **10**: 2535
[22] a) Trull FR, Shrout DP, Lightner DA (1992) Tetrahedron **48**: 8189; b) Gawroński JK, Polonski T, Lightner DA (1990) Tetrahedron **46**: 8053
[23] Kratky C, Jorde C, Falk H, Thirring K (1983) Tetrahedron **39**: 1859
[24] Sheldrick WS, Borkenstein A, Blacha-Puller M, Gaossauer A (1977) Acta Crystallogr **B33**: 3625
[25] Molecular mechanics and dynamics calculations employed to find the global energy minimum conformations of **1**, **2**, and **4** were run on an SGI Octane workstation using vers. 6.9 of the Sybyl forcefield as described in Ref. [4]
[26] Blessing R (1995) Acta Crystallogr **A51**: 33
[27] SAINT V6.1, Bruker Analytical X-ray Systems. Madison, WI, USA
[28] SHELXTL-Plus V5.10, Bruker Analytical X-ray Systems. Madison, WI, USA